Ionization of helium by intense XUV laser pulses: Numerical simulations on channel-resolved probabilities

Chuan Yu and Lars Bojer Madsen
Department of Physics and Astronomy, Aarhus University, DK-8000 Aarhus C, Denmark
(Received 8 March 2016; published 14 April 2016)

Ionization of a helium atom by intense extreme ultraviolet laser pulses is investigated in a frequency regime where the high-frequency stabilization condition is only fulfilled for the lowest single ionization channel. Multiphoton double ionization substantially contributes to the total ionization probability for superintense fields. As a result, no obvious stabilization against total ionization occurs. A detailed view of probabilities into different single ionization channels as a function of the field strength is presented. We find that the probabilities into some ionic channels peak at field strengths corresponding to one-photon resonances between field-dressed ionic states in the high-frequency Floquet theory. Thus we propose a sequential "ionization-excitation" mechanism in the dressed energy picture: first, one-photon absorption causes single ionization, leaving the ion in its dressed ground state; second, the ion is excited to a new state via one-photon absorption at the field strength where the resonance condition in the dressed ionic system is fulfilled. To reveal the sequential mechanism in the time domain, we also take a time-dependent view on the channel-resolved probabilities, observing the decrease of the ground-state ionic channel probability during the laser pulse when the field strength is such that a resonance condition exists between the dressed states in the ion.

DOI: 10.1103/PhysRevA.93.043412

I. INTRODUCTION

Strong-field ionization of atoms has been the subject of extensive theoretical and experimental investigations over decades. Developments of new light sources and focusing techniques have enabled the production of laser pulses with unprecedented high intensity. Nowadays, extreme-ultraviolet (XUV) laser pulses with femto- or subfemtosecond durations can be generated from high-order harmonics [1,2] or free electron lasers [3,4]. Such ultrashort laser pulses provide the opportunity of monitoring matter on ultrafast time scales [5–7]. Besides, new dynamics and phenomena may be induced by the extremely intense fields.

Stabilization, i.e., a decreasing trend of ionization yield with increasing laser intensity, is one of the well-known nonperturbative phenomena in strong-field ionization. It was theoretically discovered for high-frequency laser fields [8,9] and some experimental observations were reported for Rydberg atoms [10–14]. One reason for choosing Rydberg atoms as experimental targets is that the high-frequency condition can be more easily fulfilled for Rydberg atoms than for ground-state atoms. To observe stabilization, the high-frequency condition requires a single photon to have sufficient energy to ionize the atom, which for intense laser fields is defined as the stabilization regime [10]. There have been a number of theoretical studies on stabilization of one-electron systems (see review articles [15,16]). Comparatively, studies on stabilization of multielectron systems are still rare, and the research targets are mainly restricted to two-electron systems. For example, research on two-electron atoms in strong fields with the high-frequency Floquet theory (HFFT) concluded that stabilization occurs for two-electron atoms as well [17]. With a one-dimensional (1D) model of helium, the effect of electron correlation in stabilization was investigated in Ref. [18]. *Ab initio* calculations of three-dimensional (3D) helium in superintense XUV fields were reported in Refs. [19,20] and stabilization of the two-electron atom was observed in the numerical experiments.

Recently a theoretical study [21], focusing on laser-induced dynamics of the simplest molecule H_2^+ in the XUV regime, reported that highly nonresonant dissociation can dominate over ionization when stabilization occurs. Reference [21] also briefly discussed the possible extension of the mechanism to other molecules. In contrast to single-electron systems like H_2^+, the existence of electron correlation in multielectron systems increases the complexity of laser-induced dynamics and causes great interest in revealing its roles in strong-field phenomena [22–24]. In the stabilization regime, theoretical studies for two-electron atoms have indicated that electron correlation can suppress the stabilization effect [18–20]. This conclusion is reached by comparing the total ionization (TI) probabilities obtained from calculations including electron correlation with those obtained from independent-electron model calculations. For a two-electron system, TI means the sum of single ionization (SI) and double ionization (DI), and SI contains contributions from many ionic channels, i.e., the ion can be left in the ground state or some excited states. As a consequence, a two-electron system has multiple ionization energies, i.e., it has SI thresholds in different ionic channels and a DI threshold. One may consider a photon energy that is only larger than the lowest ionization energy. In this case only one channel is in the stabilization regime, while multiphoton ionization into other channels is possible. The frequency regime considered in this work is illustrated in Fig. 1 with some energy levels of He. The physics discussed is similar to that for multielectron molecular systems, e.g., H_2. Previous studies of stabilization in two-electron atoms [18–20] focused on TI, SI, and DI probabilities. To our knowledge, there has been no detailed view on ionization probabilities of different ionic channels under such strong-field conditions. In this work we take a look at the probabilities of reaching different ionic channels when a helium atom is ionized by an intense XUV laser pulse, and show that channel-resolved probabilities provide more information about strong-field ionization. On the basis of the field-dressed energy levels in the HFFT [15,25],

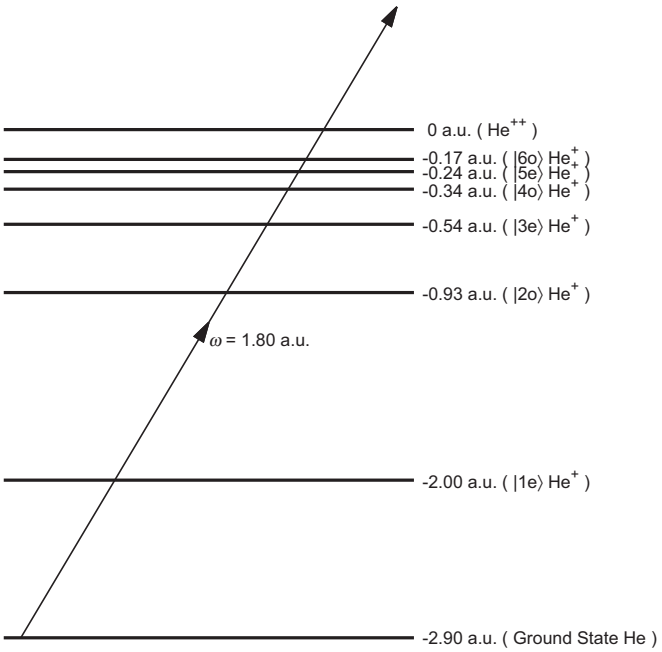

FIG. 1. Laser frequency regime considered in this work, illustrated with some energy levels of a 1D model of helium (see the text in Sec. II). The stabilization condition is fulfilled for the ground-state ionic channel labeled as $|1e\rangle$ He^+, but not for the rest of the channels.

we identify an "ionization-excitation" sequential mechanism in the considered frequency regime.

This paper is organized as follows. In Sec. II we introduce the theoretical and numerical methods used in this work. In Sec. III we present and discuss the results of the calculations. Finally we give concluding remarks in Sec. IV. Atomic units are used throughout.

II. THEORETICAL MODEL AND METHODS

We consider a 1D model of helium in the presence of a linearly polarized laser pulse, in which the two electrons are allowed to move along the direction of the laser polarization. This 1D model reduces computational difficulty, and allows us to perform calculations for a wide range of laser parameters, which is essential for the questions addressed in this work. We numerically solve the time-dependent Schrödinger equation (TDSE)

$$i\partial_t \Psi(x_1,x_2,t) = \hat{H}(t)\Psi(x_1,x_2,t), \tag{1}$$

with the Hamiltonian

$$\hat{H}(t) = \sum_{j=1}^{2}\left[\frac{\hat{p}_j^2}{2} + A(t)\hat{p}_j + V_{\rm en}(x_j)\right] + V_{\rm ee}(x_1,x_2). \tag{2}$$

Here x_j and $\hat{p}_j = -i\partial_{x_j}$ $(j = 1,2)$ are the electron coordinates and momenta, respectively, and

$$V_{\rm en}(x_j) = \frac{-2}{\sqrt{x_j^2 + a_{\rm en}}} \quad (j = 1,2), \tag{3}$$

$$V_{\rm ee}(x_1,x_2) = \frac{1}{\sqrt{(x_1 - x_2)^2 + a_{\rm ee}}} \tag{4}$$

are the electron-nuclei interaction and the electron-electron interaction, where $a_{\rm en}$ and $a_{\rm ee}$ are softening parameters used to avoid the Coulomb singularity. The laser interaction is described in velocity gauge by the vector potential $A(t)$ within dipole approximation, and a time-dependent energy shift from the $A^2(t)$ term in the Hamiltonian has been unitarily transformed away. In our calculations, a vector potential with a Gaussian envelope is used:

$$A(t) = \frac{F_0}{\omega}\exp\left(-4\ln 2\frac{t^2}{\tau^2}\right)\sin(\omega t), \tag{5}$$

where F_0 is the maximum field strength related to the peak intensity by $I = F_0^2$, ω is the angular frequency, and τ is the full width at half maximum (FWHM) of the envelope. The pulse duration is described by the number of cycles within $\tau, N_c = \omega\tau/(2\pi)$.

We express the Hamiltonian and the wave function in a finite-element discrete variable representation (FEDVR) [26,27] basis set, and solve the TDSE with the Arnoldi-Lanczos time propagator [28,29]. The initial wave function is obtained by imaginary time propagation [30]. By choosing softening parameters $a_{\rm en} = 0.50$ and $a_{\rm ee} = 0.33$, we obtain the He ground-state energy -2.90 and He^+ ionic ground-state energy -2.00, which are both good approximations to the values for the 3D systems.

The time-dependent surface flux (t-SURFF) method [31,32] allows one to extract photoelectron spectra (PES) by moniter-ing electron flux through some surfaces (see also Ref. [33] for an extension of the t-SURFF method to the molecular case and Refs. [34,35] for other recent applications). So the PES is calculated with good accuracy, and at the same time the outgoing flux is absorbed to avoid unphysical reflections at the boundaries of the simulation box. The advantage of the t-SURFF method is that we can obtain the PES with a relatively small simulation box. In our work, a complex absorbing potential (CAP) [36]

$$V_{\rm CAP}(x_1,x_2) = -i[f_{\rm CAP}(x_1) + f_{\rm CAP}(x_2)] \tag{6}$$

is added to the Hamiltonian in real time propagation, where $f_{\rm CAP}(x)$ is a function of the form

$$f_{\rm CAP}(x) = \begin{cases} 1 - \cos\left[\frac{\pi(|x|-r_c)}{2(r_{\rm max}-r_c)}\right], & r_c < |x| < r_{\rm max}, \\ 0, & |x| \leqslant r_c. \end{cases} \tag{7}$$

We set up a simulation box $r_{\rm max} = 120$ with 120 equal-size finite elements and 9 DVR basis functions in each element. The t-SURFF surfaces are placed at $|x_1|,|x_2| = 60$ and the CAP radius is $r_c = 65$. In real time propagation, we use a time step of $\Delta t = 0.005$. The convergence is checked with computations using a larger box ($r_{\rm max} = 150$ with 150 finite elements, the t-SURFF surfaces placed at $|x_1|,|x_2| = 80$, and the CAP radius $r_c = 85$).

For SI, the PES $S_{{\rm SI},c}(E_1)$ describes the probability in which one electron is freed with energy E_1 and the ion is in state c (SI channel c). The eigenstates of He^+, which are essential for calculating $S_{{\rm SI},c}(E_1)$, are obtained by diagonalizing the ionic Hamiltonian in the FEDVR basis. For DI, the PES $S_{\rm DI}(E_1,E_2)$ describes the probability in which two electrons are freed with energy E_1 and E_2. A detailed discussion of the t-SURFF method used for calculating $S_{{\rm SI},c}(E_1)$ and $S_{\rm DI}(E_1,E_2)$ can be

found in Ref. [32]. With the PES $S_{\mathrm{SI},c}(E_1)$ and $S_{\mathrm{DI}}(E_1,E_2)$, the probabilities for SI channel c and DI are readily obtained,

$$P_{\mathrm{SI},c} = \int S_{\mathrm{SI},c}(E_1)dE_1, \tag{8}$$

$$P_{\mathrm{DI}} = \iint S_{\mathrm{DI}}(E_1,E_2)dE_1dE_2. \tag{9}$$

Since the outgoing flux is absorbed by the CAP, we describe the total ionization probability as

$$P_{\mathrm{TI}} = 1 - \iint_{|x_1|,|x_2|\leqslant 60} |\Psi(x_1,x_2,t\to\infty)|^2 dx_1dx_2, \tag{10}$$

where the integral is restricted to the inner region defined by the t-SURFF surfaces. The inner region should be much larger than the amplitude of the electron quiver motion, which is essential for the theoretical methods used in this work. Notice that the largest quiver radius $\alpha_0 = F_0/\omega^2$ in our calculations is $\approx$3, which is much smaller than the extent of the inner region.

Due to the 1D model used here, a given electronic state wave function can be classified as even or odd. For the ion He^+, we use the notations $|1e\rangle$, $|2o\rangle$, $|3e\rangle$, $|4o\rangle$, ..., for the ground state and the excited states. These notations are also used later for dressed energy levels [see Eq. (15) in Sec. III]. The eigenstates of the dressed He^+ are also obtained by diagonalizing the corresponding Hamiltonian in the FEDVR basis.

III. RESULTS AND DISCUSSION

Figure 2 shows SI, DI, and TI probabilities versus field strength F_0, for fixed $\omega = 1.80$ and $N_c = 20$. The TI and DI probabilities are calculated with Eqs. (10) and (9), respectively; and then the SI probability is obtained by $P_{\mathrm{SI}} = P_{\mathrm{TI}} - P_{\mathrm{DI}}$. In the considered frequency regime, only the $|1e\rangle$ He^+ channel is open by one-photon absorption, while two-photon absorption can open all the SI channels and the DI channel, as shown in

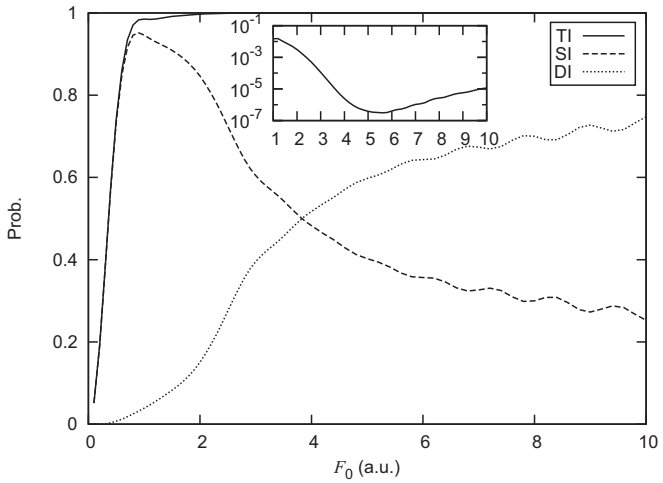

FIG. 2. SI (dashed line), DI (dotted line), and TI (solid line) probabilities of ground-state helium vs field strength F_0, for a 20-cycle pulse with $\omega = 1.80$. Inset: log-scale plot of bound probability $(1 - P_{\mathrm{TI}})$ for field strengths $1.0 \leqslant F_0 \leqslant 10.0$, with its minimum corresponding to the maximum TI probability.

Fig. 1. The behavior of these probabilities can be roughly classified into three regimes. First, for low field strengths ($F_0 < 1.0$), P_{TI} increases dramatically with F_0 and the main contribution is from SI. At $F_0 = 1.0$, P_{TI} is quite high (> 0.9). Second, with increasing field strength $1.0 < F_0 < 5.5$, DI starts to contribute and P_{SI} decreases. There is also a small increase in P_{TI} (see the inset of Fig. 2). Third, for very strong fields ($F_0 > 5.5$), both SI and DI probabilities vary slowly with F_0 and show a small oscillating behavior. The oscillating behavior in the ionization probability was reported and discussed for one-electron models [37,38], and is not the focus of the present work. From the inset of Fig. 2, one finds a slight decreasing trend in P_{TI} in this very high field-strength regime.

Considering the laser frequency $\omega = 1.80$, there exists a decreasing trend in the SI probability with increasing field strength. However, the DI probability increases with increasing field strength, indicating that the atom is not actually stabilized. In extremely intense fields, one finds that multiphoton DI contributes substantially, leading to very high TI probabilities. This means that the coexistence of one-photon ionization of the lowest channel, which is in the stabilization regime, and multiphoton ionization into other channels results in no obvious stabilization against TI. So the mechanism of dissociation proposed in Ref. [21] may not be observed for multielectron molecules in the laser frequency regime considered here. In Ref. [18], it was also concluded that stabilization would not be achieved in such an intermediate frequency regime and that the slight decreasing trend in the TI probability should not be seen as real stabilization. Our results, however, can provide more information about the ionization in different channels (see also the later discussion). In addition, we have performed calculations for 20-cycle laser pulses with frequency $\omega = 4.00$, which is above the DI threshold. Our results for $\omega = 4.00$ (not shown) are similar to those obtained from numerical simulations of 3D He [19], i.e., stabilization against TI is clearly observed. This conclusion agrees with Ref. [18] as well. It implies that the mechanism of dissociation proposed in Ref. [21] may be observed for multielectron molecules, if the laser frequency is high enough to cause substantial stabilization in all the ionization channels.

In Fig. 3(a) we take a detailed view on the lowest eight SI channels contributing to the dashed curve in Fig. 2. For comparison, we perform calculations for a 20-cycle pulse with a lower frequency $\omega = 1.70$, and present the results in Fig. 3(b). As seen from Figs. 3(a) and 3(b), the lowest eight SI channels comprise the majority of the SI probability ($> 67\%$ over the considered field strength range) and show some representative behaviors. In both Figs. 3(a) and 3(b), we find that all the even-wave-function channels, except the $|1e\rangle$ He^+ channel, contribute little to the SI probability over the considered field strength range. For low field strengths, the $|1e\rangle$ He^+ channel dominates the SI probability (compare $P_{\mathrm{SI},|1e\rangle}$ with P_{SI} in Fig. 3). In Fig. 3(a), $P_{\mathrm{SI},|1e\rangle}$ increases with the field strength up to $F_0 = 0.5$; after that it shows some oscillations and an overall decreasing trend. In Fig. 3(a), one can also find interesting peaks of $P_{\mathrm{SI},|6o\rangle}$ and $P_{\mathrm{SI},|8o\rangle}$ at $F_0 = 1.1$ and $F_0 = 1.8$, respectively. For $\omega = 1.70$, similar peaks of $P_{\mathrm{SI},|4o\rangle}$, $P_{\mathrm{SI},|6o\rangle}$, and $P_{\mathrm{SI},|8o\rangle}$ appear in Fig. 3(b). There is a common feature that these channels are odd-wave-function

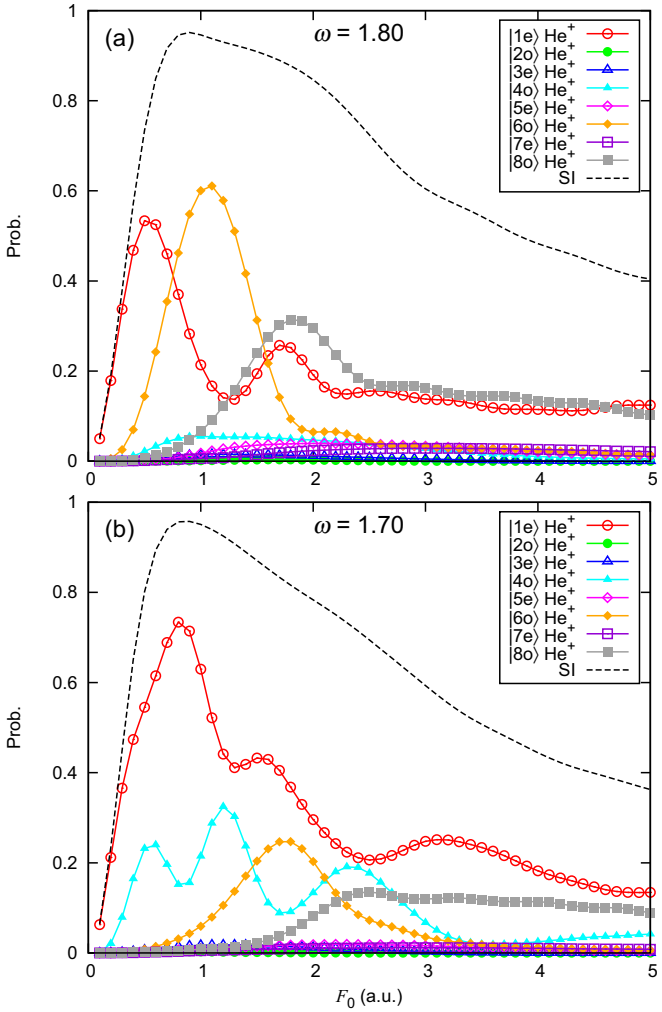

FIG. 3. (a) Probabilities of the lowest eight SI channels (solid lines in different colors) vs field strength F_0, for a 20-cycle pulse with $\omega = 1.80$. The SI probability vs F_0 is plotted with dashed line (the same as Fig. 2). (b) Results for a 20-cycle pulse with $\omega = 1.70$.

ionic states. Also, the probability of a higher ionic channel peaks at a larger field strength. To understand these notable peaks, we resort to the Kramer-Henneberger (KH) frame [39] and dressed energy levels on the basis of the lowest-order HFFT [25].

By applying a space translation $\alpha(t) = \int^t A(t')dt'$ to the electron coordinates x_1 and x_2 in Eqs. (1) and (2), the TDSE and the Hamiltonian in the KH frame are obtained,

$$i\partial_t \Phi_{\rm KH}(x_1,x_2,t) = \hat{H}_{\rm KH}(t)\Phi_{\rm KH}(x_1,x_2,t), \tag{11}$$

$$\hat{H}_{\rm KH}(t) = \sum_{j=1}^{2}\left[\frac{\hat{p}_j^2}{2} + V_{\rm en}[x_j+\alpha(t)]\right] + V_{\rm ee}(x_1,x_2). \tag{12}$$

The use of the KH frame is essential for the formulation of the HFFT. Note that in our calculations, we do not perform real time propagation of the TDSE in the KH frame, so there is no absorbing boundary such as Eq. (6) used in the KH frame.

In the long-pulse limit, with $\alpha_0 = F_0/\omega^2$, the quiver motion can be simply expressed as $\alpha(t) = \alpha_0\cos(\omega t)$. We then perform a Fourier expansion of the oscillating potential $V_{\rm en}$,

$$V_{\rm en}[x_j + \alpha_0\cos(\omega t)] = \sum_n V_n(\alpha_0,x_j)\exp(-in\omega t) \quad (j = 1,2). \tag{13}$$

The zeroth components $V_0(\alpha_0,x_1)$ and $V_0(\alpha_0,x_2)$, together with $V_{\rm ee}(x_1,x_2)$, represent the time-averaged potential in the presence of high-frequency laser fields, which is called the dressed potential in the HFFT [15,25]. Considering a laser pulse, we see α_0 as a time-dependent quantity varying with the pulse envelope and assume that the dressed energy levels follow the pulse envelope (see the discussion below).

To the lowest order, the HFFT gives the structure equation [15,25],

$$\left\{\sum_{j=1}^{2}\left[\frac{\hat{p}_j^2}{2} + V_0(\alpha_0,x_j)\right] + V_{\rm ee}(x_1,x_2)\right\}\Phi(x_1,x_2) = W(\alpha_0)\Phi(x_1,x_2). \tag{14}$$

Similarly, the structure equation for the He^+ ion reads

$$\left[\frac{\hat{p}^2}{2} + V_0(\alpha_0,x)\right]\Phi_c(x) = W_c(\alpha_0)\Phi_c(x). \tag{15}$$

We solve Eqs. (14) and (15), and plot some selected dressed energy levels in Figs. 4(a) and 4(b) for the two frequencies $\omega = 1.80$ and $\omega = 1.70$.

With increasing field strength, the rise of the ground-state He energy and the $|1e\rangle$ He^+ energy can be clearly observed in Fig. 4, while the energy shifts of higher ionic states are less pronounced. With one photon energy, the dressed $|1e\rangle$ He^+ state can be coupled with dressed odd-wave-function ionic states at resonance for some specific field strengths. Here we also consider the spectral width of the laser pulses, as the dotted curves in Fig. 4 indicate.

On the basis of these dressed energy levels, we propose a sequential "ionization-excitation" mechanism to understand the notable peaks in probabilities of some odd-wave-function ionic channels in Fig. 3. We take the peak of $P_{{\rm SI},|6o\rangle}$ at $F_0 = 1.1$ in Fig. 3(a) as an illustrative example. First, the ground-state He atom is ionized into the $|1e\rangle$ He^+ channel, which is the dominant process for low field strengths. For $\omega = 1.80$, there exists a resonance condition between the $|1e\rangle$ He^+ and $|6o\rangle$ He^+ states on the dressed energy levels, around the field strength $F_0 = 1.1$. Such a resonance allows the dressed $|1e\rangle$ He^+ to be efficiently excited to the dressed $|6o\rangle$ He^+ with one-photon absorption mediated to the lowest order by the $n = \pm 1$ terms in Eq. (13). With the assumption that the system can adiabatically follow the dressed energy levels, the resonant excitation from the dressed $|1e\rangle$ He^+ to the dressed $|6o\rangle$ He^+ can explain the decrease of $P_{{\rm SI},|1e\rangle}$ and the increase of $P_{{\rm SI},|6o\rangle}$. It can be seen from Fig. 3(a) that $P_{{\rm SI},|6o\rangle}$ is much higher than $P_{{\rm SI},|1e\rangle}$ at the field strength $F_0 = 1.1$. A view of $P_{{\rm SI},|1e\rangle}$ and $P_{{\rm SI},|6o\rangle}$ in the time domain will be discussed later in this paper. Similarly, the sequential ionization-excitation mechanism can also explain the peak of $P_{{\rm SI},|8o\rangle}$ at $F_0 = 1.8$ in Fig. 3(a). The field strength corresponding to the $P_{{\rm SI},|8o\rangle}$ peak is larger than that corresponding to the $P_{{\rm SI},|6o\rangle}$ peak, since the resonance condition between the dressed $|1e\rangle$ He^+ and $|8o\rangle$ He^+ states appears at a larger field strength F_0.

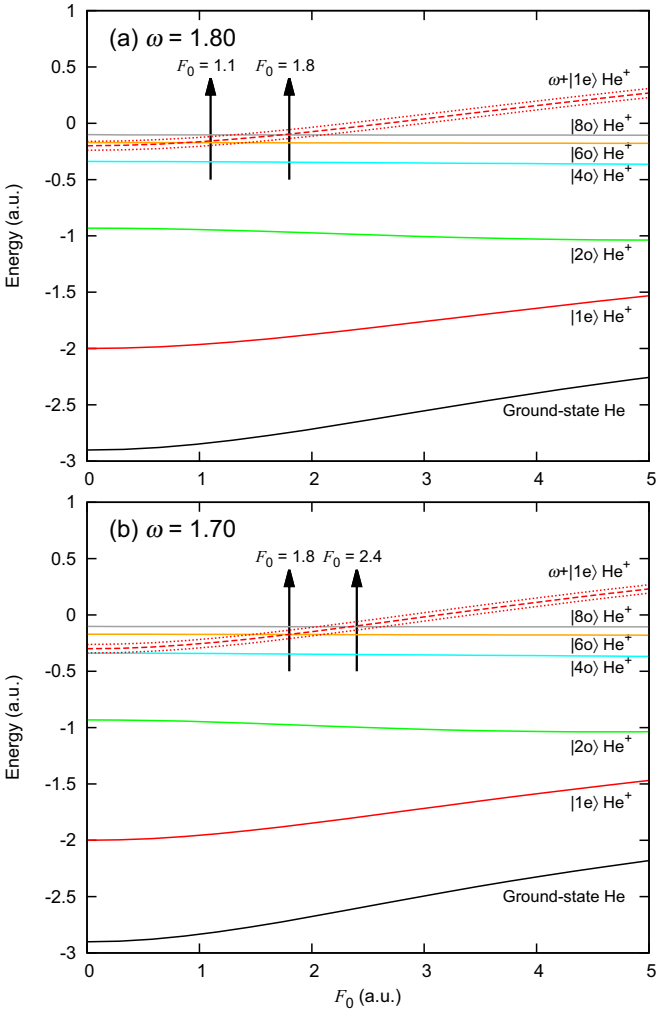

FIG. 4. Dressed energy levels vs field strength F_0 for laser frequencies (a) $\omega = 1.80$ and (b) $\omega = 1.70$. The solid curves, from bottom to top, correspond to ground-state He (black line), $|1e\rangle$ He^+ (red line), $|2o\rangle$ He^+ (green line), $|4o\rangle$ He^+ (cyan line), $|6o\rangle$ He^+ (orange line), and $|8o\rangle$ He^+ (gray line). The dashed red and dotted red curves are $W_{|1e\rangle} + \omega$ and $W_{|1e\rangle} + \omega \pm \Delta\omega$, respectively. Here $\Delta\omega$ is the FWHM in frequency domain for a 20-cycle pulse, and $W_{|1e\rangle}$ is the dressed ionic ground-state energy [see Eq. (15)]. The arrows indicate the field strengths corresponding to the peaks of $P_{\mathrm{SI},|6o\rangle}$ and $P_{\mathrm{SI},|8o\rangle}$ in Fig. 3.

Turning attention to Fig. 4(b), for $\omega = 1.70$, one finds that the resonance conditions between the dressed $|1e\rangle$ He^+ and $|6o\rangle$ He^+ states and between the dressed $|1e\rangle$ He^+ and $|8o\rangle$ He^+ states agree well with the $P_{\mathrm{SI},|6o\rangle}$ peak and the $P_{\mathrm{SI},|8o\rangle}$ peak in Fig. 3(b). Although we cannot completely explain the complicated behavior of $P_{\mathrm{SI},|4o\rangle}$ in Fig. 3(b), the large yields of $|4o\rangle$ He^+ at low field strengths are reasonable since the one-photon excitation from the $|1e\rangle$ He^+ state to the $|4o\rangle$ He^+ state exists at low field strengths, as Fig. 4(b) indicates.

In the above discussion, the sequential ionization-excitation mechanism based on the dressed energy levels should be understood as the main contribution to some specific SI channels. In the dressed energy picture, all the possible transitions between the dressed states occur together with the adiabatic following of the dressed states. In fact, the sequential ionization-excitation mechanism proposed here is only part of the complicated dynamics, and it becomes prominent for some specific laser parameters.

We perform an additional investigation about this sequential mechanism by taking a time-dependent view on the channel-resolved probabilities at two selected field strengths showing representative behaviors, as Fig. 5 displays. All the time sampling points t_s in Fig. 5 correspond to $A(t_s) = 0$. To obtain the channel-resolved probabilities at each time sampling point t_s, we turn off the laser interaction from t_s by simply replacing $A(t)$ with $\theta(t_s - t)[A(t) - A(t_s)]$ in the time-dependent Hamiltonian [40], and carry out real time propagation with the t-SURFF method as mentioned in Sec. II. For a field strength of $F_0 = 0.5$, both $P_{\mathrm{SI},|1e\rangle}$ and $P_{\mathrm{SI},|6o\rangle}$ increase with time during the pulse, and $P_{\mathrm{SI},|1e\rangle}$ is much larger. This field strength $F_0 = 0.5$ corresponds to the peak of $P_{\mathrm{SI},|1e\rangle}$ in Fig. 3(a). For a field strength of $F_0 = 1.1$, $P_{\mathrm{SI},|1e\rangle}$ grows with time in the beginning, then it starts to decrease around the center of the pulse. Meanwhile, $P_{\mathrm{SI},|6o\rangle}$ shows a dramatic increase with time during the pulse. This field strength $F_0 = 1.1$ corresponds to the peak of $P_{\mathrm{SI},|6o\rangle}$ in Fig. 3(a). The decrease of $P_{\mathrm{SI},|1e\rangle}$ around the center of the pulse reflects the excitation from the $|1e\rangle$ He^+ state to the $|6o\rangle$ He^+ state in the dressed energy picture.

In closing this section, we mention that strong-field phenomena induced by near-infrared (NIR) laser pulses in multielectron systems have attracted considerable interest over decades [22–24]. In the NIR regime, both ionization and excitation are usually multiphoton processes, so there is hardly any one-photon resonance condition between the involved states. Unlike in the XUV regime where the coupling between only a few states can be easily identified with one-photon resonance conditions, in the NIR regime many states may be coupled with each other via multiphoton processes, resulting in more complicated dynamics.

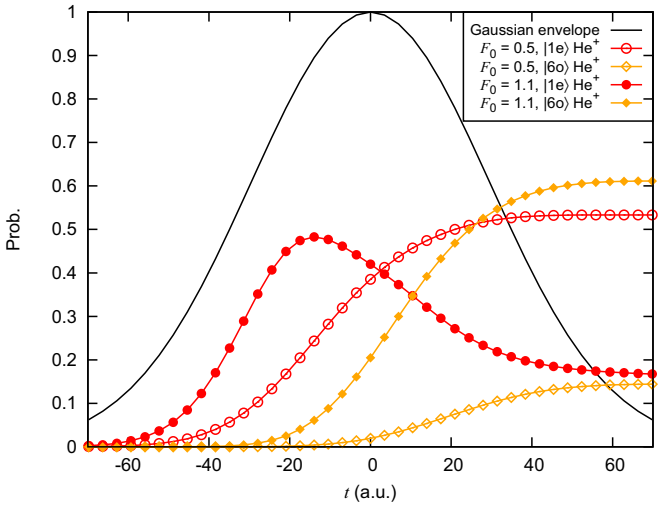

FIG. 5. Time-dependent view of $P_{\mathrm{SI},|1e\rangle}$ (red lines) and $P_{\mathrm{SI},|6o\rangle}$ (orange lines) for a 20-cycle pulse with frequency $\omega = 1.80$, at two different field strengths $F_0 = 0.5$ and $F_0 = 1.1$. The Gaussian envelope (with maximum set to 1) is also plotted with solid black line.

IV. CONCLUSION

In this paper, we studied the ionization of He by intense XUV laser pulses by performing numerical simulations. We considered a frequency regime where the lowest SI channel is expected to be stabilized and ionization into other channels requires absorption of two or more photons, as illustrated in Fig. 1. We found that there is no obvious stabilization against TI in this frequency regime, due to large yields of multiphoton DI for superintense fields. We took a detailed view of probabilities into different SI channels as a function of the field strength, observing interesting peaks of probabilities into some odd-wave-function ionic states. To our knowledge, such research on channel-resolved ionization probabilities has not been reported previously. We showed that it can decode more information about strong-field ionization of multielectron systems. From the dressed energy levels based on the lowest order HFFT, we found one-photon resonance conditions between the dressed ionic ground state and excited states at the field strengths corresponding to those peaks. Thus we proposed a sequential ionization-excitation mechanism in the dressed energy picture: after the atom is singly ionized into the lowest ionic channel, the ion is further excited to another state at the field strength where the resonance condition between the dressed ionic states is fulfilled. Finally, a time-dependent view of the channel-resolved probabilities was also presented to further reveal the proposed sequential mechanism.

ACKNOWLEDGMENTS

This work was supported by the European Research Council StG (Project No. 277767-TDMET), and the VKR center of excellence, QUSCOPE. The numerical results presented in this work were performed at the Centre for Scientific Computing, Aarhus.

[1] G. Sansone, L. Poletto, and M. Nisoli, High-energy attosecond light sources, Nat. Photon. **5**, 655 (2011).

[2] M. Chini, K. Zhao, and Z. Chang, The generation, characterization and applications of broadband isolated attosecond pulses, Nat. Photon. **8**, 178 (2014).

[3] W. Ackermann, G. Asova, V. Ayvazyan, A. Azima, N. Baboi, J. Bähr, V. Balandin, B. Beutner, A. Brandt, A. Bolzmann *et al.*, Operation of a free-electron laser from the extreme ultraviolet to the water window, Nat. Photon. **1**, 336 (2007).

[4] B. W. McNeil and N. R. Thompson, X-ray free-electron lasers, Nat. Photon. **4**, 814 (2010).

[5] M. Hentschel, R. Kienberger, C. Spielmann, G. Reider, N. Milosevic, T. Brabec, P. Corkum, U. Heinzmann, M. Drescher, and F. Krausz, Attosecond metrology, Nature (London) **414**, 509 (2001).

[6] F. Krausz and M. I. Stockman, Attosecond metrology: From electron capture to future signal processing, Nat. Photon. **8**, 205 (2014).

[7] F. Krausz and M. Ivanov, Attosecond physics, Rev. Mod. Phys. **81**, 163 (2009).

[8] M. Fedorov and A. Movsesian, Field-induced effects of narrowing of photoelectron spectra and stabilisation of Rydberg atoms, J. Phys. B **21**, L155 (1988).

[9] M. Pont and M. Gavrila, Stabilization of Atomic Hydrogen in Superintense, High-frequency Laser Fields of Circular Polarization, Phys. Rev. Lett. **65**, 2362 (1990).

[10] M. P. de Boer, J. H. Hoogenraad, R. B. Vrijen, L. D. Noordam, and H. G. Muller, Indications of High-intensity Adiabatic Stabilization in Neon, Phys. Rev. Lett. **71**, 3263 (1993).

[11] R. R. Jones, D. W. Schumacher, and P. H. Bucksbaum, Population trapping in Kr and Xe in intense laser fields, Phys. Rev. A **47**, R49 (1993).

[12] M. P. de Boer, J. H. Hoogenraad, R. B. Vrijen, R. C. Constantinescu, L. D. Noordam, and H. G. Muller, Adiabatic stabilization against photoionization: An experimental study, Phys. Rev. A **50**, 4085 (1994).

[13] J. H. Hoogenraad, R. B. Vrijen, and L. D. Noordam, Ionization suppression of Rydberg atoms by short laser pulses, Phys. Rev. A **50**, 4133 (1994).

[14] N. J. van Druten, R. C. Constantinescu, J. M. Schins, H. Nieuwenhuize, and H. G. Muller, Adiabatic stabilization: Observation of the surviving population, Phys. Rev. A **55**, 622 (1997).

[15] M. Gavrila, Atomic stabilization in superintense laser fields, J. Phys. B **35**, R147 (2002).

[16] A. M. Popov, O. V. Tikhonova, and E. A. Volkova, Strong-field atomic stabilization: Numerical simulation and analytical modelling, J. Phys. B **36**, R125 (2003).

[17] M. Gavrila and J. Shertzer, Two-electron atoms in superintense radiation fields: Dichotomy and stabilization, Phys. Rev. A **53**, 3431 (1996).

[18] D. Bauer and F. Ceccherini, Electron correlation versus stabilization: A two-electron model atom in an intense laser pulse, Phys. Rev. A **60**, 2301 (1999).

[19] T. Birkeland, R. Nepstad, and M. Førre, Stabilization of Helium in Intense XUV Laser Fields, Phys. Rev. Lett. **104**, 163002 (2010).

[20] S. A. Sørngård, S. Askeland, R. Nepstad, and M. Førre, Multiphoton ionization and stabilization of helium in superintense XUV fields, Phys. Rev. A **83**, 033414 (2011).

[21] L. Yue and L. B. Madsen, Characterization of Molecular Breakup by Very Intense Femtosecond XUV Laser Pulses, Phys. Rev. Lett. **115**, 033001 (2015).

[22] W. Becker and H. Rottke, Many-electron strong-field physics, Contemp. Phys. **49**, 199 (2008).

[23] C. F. de Morisson Faria and X. Liu, Electron electron correlation in strong laser fields, J. Mod. Opt. **58**, 1076 (2011).

[24] W. Becker, X. Liu, P. J. Ho, and J. H. Eberly, Theories of photoelectron correlation in laser-driven multiple atomic ionization, Rev. Mod. Phys. **84**, 1011 (2012).

[25] M. Gavrila, *Atoms in Intense Laser Fields* (Academic Press, San Diego, 1992).

[26] T. N. Rescigno and C. W. McCurdy, Numerical grid methods for quantum-mechanical scattering problems, Phys. Rev. A **62**, 032706 (2000).

[27] B. I. Schneider, L. A. Collins, and S. X. Hu, Parallel solver for the time-dependent linear and nonlinear Schrödinger equation, Phys. Rev. E **73**, 036708 (2006).

[28] T. J. Park and J. C. Light, Unitary quantum time evolution by iterative Lanczos reduction, J. Chem. Phys. **85**, 5870 (1986).

[29] X. Guan, O. Zatsarinny, K. Bartschat, B. I. Schneider, J. Feist, and C. J. Noble, General approach to few-cycle intense laser interactions with complex atoms, Phys. Rev. A **76**, 053411 (2007).

[30] R. Kosloff and H. Tal-Ezer, A direct relaxation method for calculating eigenfunctions and eigenvalues of the Schrödinger equation on a grid, Chem. Phys. Lett. **127**, 223 (1986).

[31] L. Tao and A. Scrinzi, Photo-electron momentum spectra from minimal volumes: the time-dependent surface flux method, New J. Phys. **14**, 013021 (2012).

[32] A. Scrinzi, t-SURFF: Fully differential two-electron photo-emission spectra, New J. Phys. **14**, 085008 (2012).

[33] L. Yue and L. B. Madsen, Dissociation and dissociative ionization of H_2^+ using the time-dependent surface flux method, Phys. Rev. A **88**, 063420 (2013).

[34] A. Karamatskou, S. Pabst, Y.-J. Chen, and R. Santra, Calculation of photoelectron spectra within the time-dependent configuration-interaction singles scheme, Phys. Rev. A **89**, 033415 (2014).

[35] A. Zielinski, V. P. Majety, and A. Scrinzi, Double photoelectron momentum spectra of helium at infrared wavelength, Phys. Rev. A **93**, 023406 (2016).

[36] J. Muga, J. Palao, B. Navarro, and I. Egusquiza, Complex absorbing potentials, Phys. Rep. **395**, 357 (2004).

[37] Q. Su, B. P. Irving, and J. H. Eberly, Ionization modulation in dynamic stabilization, Laser Phys. **7**, 568 (1997).

[38] M. Dörr and R. M. Potvliege, Adiabatic stabilization in photodetachment by ultrashort pulses, J. Phys. B **33**, L233 (2000).

[39] W. C. Henneberger, Perturbation Method for Atoms in Intense Light Beams, Phys. Rev. Lett. **21**, 838 (1968).

[40] L. B. Madsen and D. Dimitrovski, Time-resolved subcycle dynamics: Importance of physical fields and gauge invariance, Phys. Rev. A **78**, 023403 (2008).